Simulation of Magnetrons and Crossed-Field Amplifiers

GEORGE E. DOMBROWSKI

Abstract—**This paper describes a computer program for simulation of the magnetron oscillator and crossed-field amplifiers. Emphasis is placed on accuracy and efficient computation with moderate numbers of electrons and moderately large time steps. Distinctive features are 1) space-charge field evaluation by Buneman's cycle reduction method and separate treatment of electrons near the cathode; 2) circuit field and electronic induction calculation by use of a Ramo (Green's) function, accounting for space-harmonics; 3) calculation of RF network reponse by means of Green's functions; 4) predictor/corrector evaluation of average RF signals; and 5) use of fifth-degree power series calculation of electron trajectories. The simulation is illustrated in the starting of oscillations from computer noise.**

I. Introduction

EARLY attempts [1] to apply the self-consistent method of Hartree to magnetron analysis disclosed the critical dependence of trajectories on estimated fields and the converse dependence of fields on trajectories. It proved virtually impossible to obtain truly self-consistent space-charge configurations. This peculiarity of crossed-field interaction proved frustrating even with the advent of modern computers [2].

To escape this dilemma, Buneman [3] originated a "transience" calculation in which self-consistency is assured by allowing the electron stream to develop in time under the influence of an RF rotating wave. The steady state was successfully attained. This calculation appears to have been the first simulation of the electron stream in the oscillating magnetron.

In recognition of this, the author [4] extended the simulation to the behavior of the RF systems as well, enabling analysis of the magnetron oscillator and various amplifier configurations. The simulation calculation—as far as it is feasible—permits the elimination of a host of restrictive assumptions. The mode of interaction need not be presumed. The rotating wave hypothesis, which ignores the effect of the nonsynchronous half of the RF standing wave, is no longer necessary. Other space harmonics can be taken into account, as well as the penetration of electrons into the gaps between anode electrodes.

In recent years the simulation calculation has been improved by the adoption of a new algorithm for solution of Poisson's equation and other refinements. Attention has been given to reduction of computer "noise" to allow simulation under the extremely low RF signals of the onset of oscillation. The computer coding has also been made more efficient, allowing use of small computers as well as larger machines. This simulation program and its use are described below.

Manuscript received April 9, 1988; revised July 28, 1988.
The author is at 69 Birchwood Heights Road, Storrs, CT 06268.
IEEE Log Number 8823883.

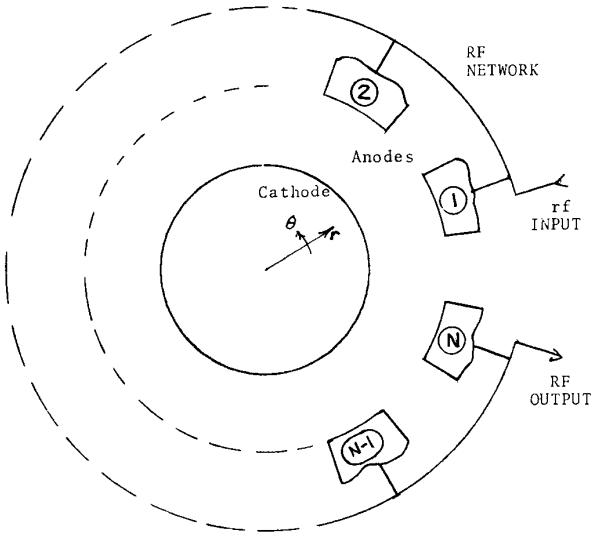

Fig. 1. Schematic diagram of interaction region and RF network.

II. Formulation

The interaction space is shown in Fig. 1 for this two-dimensional analysis. In addition to an applied anode–cathode voltage (which may be pulsed) and an applied static magnetic field, each of the anode segments may have an RF voltage by virtue of its connection to an RF network. The task of the simulation is to evaluate the electric fields of these sources and of the space-charge itself, to determine the resulting electronic motion, and to determine the effects of such motion on the RF network. Concurrently, cathode emission may take place as determined by these fields.

III. Program Description

Fig. 2 is a flow chart of the principal portions of the simulation process. The central column describes computations performed on two data bases, viz., the stream ensemble and the electrical state of the RF network. Space does not permit a detailed description; the commentary presented below merely highlights important considera-

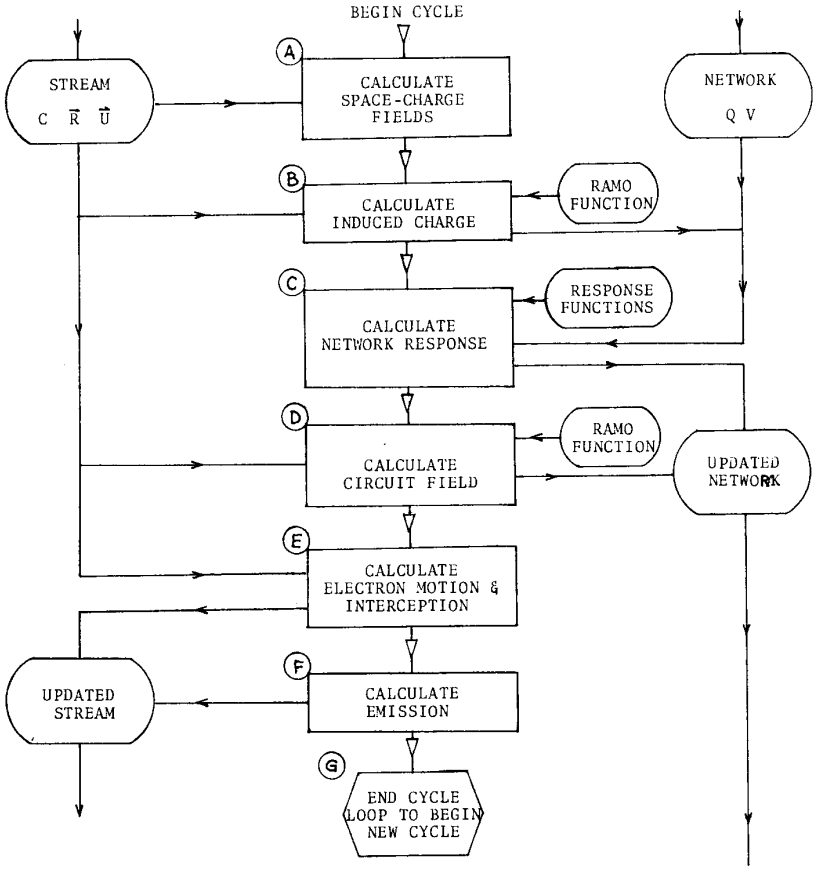

Fig. 2. Flow chart of the simulation program. Closed arrows show flow of computation; open arrows show data paths.

tions for each of the steps identified by letter (A–G) in Fig. 2.

A. Space-Charge Fields

At one time the calculation of electron–electron forces was the most time-consuming portion of the calculation. Thanks to the speed of the Buneman cyclic reduction algorithm [5] this is no longer so. By assigning the electrons to cells in a suitably constructed mesh (the number of cells in each direction is a power of 2), the Poisson equation with azimuthally periodic boundary is rapidly solved for the space-charge potential, the gradient of which is the space-charge field. With careful charge assignment and gradient evaluation, moreover, the effects of discretization can be virtually eliminated.

The cyclic reduction method does not account for charges in the cells enclosing the cathode or anode, however. Separate treatment is provided for the charges adjacent to the cathode since they appreciably affect emission. Nothing is done for electrons adjacent to or beyond the anode (between anodes) because the space-charge forces are much smaller than the fields of the RF network.

B. Induced Charge

The charge induced on each anode electrode by the stream is computed as a first step in determining stream effect on the RF network. This is done with the aid of a previously computed Green's function $\psi_n(r, \theta)$ arising from a theorem of Ramo [6].

$$\nabla^2 \psi_n = 0, \qquad \psi_n = \begin{cases} 1 \text{ on anode } n \\ 0 \text{ on anodes } n' \neq n \\ 0 \text{ on cathode} \end{cases}$$

$$q_n = -\sum_i c_i \psi_n(r_i, \theta_i).$$

This "Ramo function" is reciprocally the same function that yields the space-charge-free potential where the electron resides, when a unit potential exists at the anode electrode (and all other anodes have zero potential).

$$E_i = -\sum_n v_n \nabla \psi_n(r_i, \theta_i).$$

Clearly, the functions for the several anodes are identical except for translation in azimuth.

Values of this Green's function are pre-computed on a fine mesh so that the structural details of the anodes are preserved. In the simulation process the mesh values are used for simple rapid interpolation. Thus, both speed and accuracy are maintained.

C. Network Response

The induced charge as a function of time is differentiated to obtain the electronically induced network currents. The response of the RF network to these currents (and input currents in the amplifier) are calculated.

Green's functions for the network—response functions—can be used here, too. Elementary analysis of the linear RF network indicates that 1) the injected current and the initial conditions $v(t_0)$ and $u(t_0) = \int^{t_0} v\,dt$ may be regarded as sources or stimuli; 2) the network state after a time Δt is the combination of the effects of the stimuli considered separately; and 3) linearity applies to each stimulus. This is formally stated as

$$v_n(t_0 + \Delta t) = \sum_{n'} \left[i_e(n')\, R_i(n, n') + v_{n'}(t_0)\, R_v(n, n') + u_{n'}(t_0)\, R_u(n, n') \right]$$

where $i_e(n')$ is the electronically injected current at anode n' during the time interval. $R_i(n, n')$ is the voltage produced at node n when a unit current is injected at node n'; it is a response function. $v_{n'}(t_0)$ is the initial RF voltage at node n'. $R_v(n, n')$ is the response function equal to the voltage at n when there is an initial unit voltage at n'. $u_{n'}(t_0)$ is the initial voltage integral $\int^{t_0} v dt$ at node n'. $R_u(n, n')$ is the response function equal to $v_n(t_0 + \Delta t)$ when a unit initial $u(n')$ exists. The summation over all n' accounts for all sources.

A similar expression yields $u_n(t_0 + \Delta t)$; it involves another set of three response functions.

The calculation of the network response functions is based on a lumped-element equivalent circuit, as typified in Fig. 3 for the magnetron (concerning which, see Appendix A). The currents entering a node consist of the electronic current i_e, the conductive current Gv, the inductive current $\Gamma u = \Gamma \int v\,dt$, and the capacitive current $Cv' = C\,dv/dt$. All of these are known but the last; Kirchoff's current law can thus be used to evaluate the derivative v'. In matrix form

$$CV' = I_e - GV - \Gamma U$$

or using the inverse capacitance matrix

$$V' = C^{-1}[I_e - GV - \Gamma U].$$

The capacitance elements are furthermore modified to account for conductive and inductive currents that depend on V' through finite difference approximations

$$C \to C + G(\Delta t/2) + \Gamma(\Delta t)^2/6.$$

The matrix inversion is performed only once; other operations are simply addition and multiplication.

Once V' is determined, integration to obtain V and U at the end of the time interval is readily performed. To obtain even greater accuracy, the simulation time interval Δt is subdivided into a large number of subintervals $\Delta t'$ for the calculation of the response functions. RF networks having response over a wide frequency range can thus be handled.

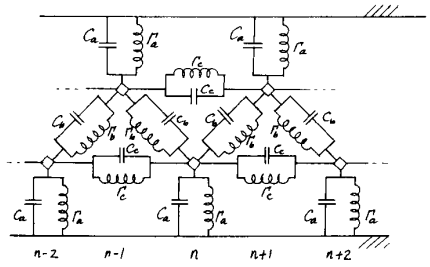

Fig. 3. General lumped-element network showing connections to the n-th anode. Conductance elements have been omitted for clarity.

Networks for representation of the magnetron oscillator and crossed-field amplifiers are discussed in Appendices A and B.

D. Circuit Field Component

As indicated above, the anode Green's function ψ is used to determine this field by interpolation from potentials. This is the most time-consuming part of the simulation, since it must be done for several hundred electrons for each of several anodes. For efficient computation the field is computed at the same time that the induced charge is reckoned.

The applicable RF anode potentials are the average values in the interval Δt. These values are not known at the start of the interval and must be estimated in advance. Largely because of the high precision of Buneman's cyclic reduction and the trajectory calculation algorithm described below, the error in estimating the average RF field—depending on the RF level—is often the greatest residual error in the simulation process. Minimization of this error allows use of relatively large time steps and thus greater computational economy. Subsequent correction is made to the RF potentials at the end of the time inverval, but this comes too late to correct the error in the fields used for trajectory calculation. Nevertheless, this error as monitored during the calculation is a small one; it is far less than involved in simpler schemes.

The space-charge and circuit components of field are added to obtain the total field. This field is strongly dependent on the electron's location. If the electron moves closer to the anode, the RF fields increase and the space-charge fields vary considerably, whether increasing or decreasing. For this reason the average fields during the time step are modified by extrapolation from the prior fields. This modification has been found useful by energy balance checks.

E. Trajectory Calculation

The electron motion is calculated by means of an analysis based on the following hypothetical steps.

1) A Cartesian coordinate system is centered at the initial electron location and aligned with the radial and azimuthal directions.

2) The coordinates and velocities in this system are expanded in power series in the cyclotron time $\omega_c t$.

3) The field vector is assumed to rotate with azimuth along the trajectory.

4) The power series coefficients are required to satisfy the equations of motion in this Cartesian system.

5) The electron position and velocity at the end of the time step are restored to the cylindrical system.

This procedure, used with fifth-degree power series, yields excellent accuracy when the cyclotron-time interval is less than a radian. The calculation can be applied iteratively for subintervals if necessary to meet this requirement. It has successfully been tested in the solid-anode diode for circular orbit conditions and for a single electron emitted under Hull cutoff conditions. The energy balance is typically better than 1 part in 10^4.

Interception at the cathode and anode is reckoned as part of the trajectory computation. Intercepted electrons are removed from the stream. In the case of anode electrons, this removal would result in a sudden decrease of induced anode charge and a corresponding pulse of anode current, neither of which has physical reality. This is avoided by assigning the intercepted charge to q_c, the collected charge, and using as the electronic current the change in the combined induced and collected charges

$$i_e = d(q_i + q_c)/dt.$$

F. Emission

At each of the cathode emitting sites the space-charge and circuit components of the potential gradient are combined as the total cathode field. If this is a retarding field, no emission takes place. Otherwise, the charge required to reduce the field to zero is computed. The emitted charge is the lesser of this charge and the emission capability of the cathode segment. This charge is assigned zero emission velocity and is merged into the stream.

G. Loop to A to Repeat Calculation for the Next Time Interval with Incremented t_0

Display of the stream and various subsidiary calculations may be performed. These include

1) space-harmonic analysis of RF anode potentials and induced charge;
2) time-harmonic analysis of anode potentials and charge;
3) energy stored in the RF network; and
4) energy dissipation and RF power output.

IV. Testing: Energy Balance

The simulation program is a large one, offering ample opportunity for error in formulation and coding. Wherever possible, program components have been tested against instances with known results.

In addition, an energy balance calculation serves as a check on the validity of the entire simulation calculation when the results are not known. The energy of the system is manifest in

1) RF network energy, in both capacitive and inductive elements;
2) electron kinetic energy; and
3) electric field energy in the stream.

Dissipative factors are

4) dissipation in the RF network (including its load) and
5) electron bombardment of the cathode and anodes.

Energy sources include

6) energy from the dc power supply;
7) in the case of the amplifier, RF input signals; and
8) in the magnetron, any locking signal.

The energy balance requires that any changes in the system energy as in items 1–3 must be provided by sources 4–8.

Under low RF conditions the energy balance is typically within 1 percent. For large signals the imbalance may be as large as 5 percent in calculations with merely 20 steps per RF cycle. The energy balance would be improved with a smaller time step.

V. Choice of Computer

The simulation calculation requires large computer memory and lengthy computation. This would indicate use of large "mainframe" high-speed computers. Certainly for "production" calculations they would be economical.

Small computers are attractive as research tools, however. Computer memory is now so cheap that size is no longer a limiting factor; their principal disadvantage is their lower speed. This is often acceptable in view of the limited ability of the researcher to assimilate the information provided by the computer. On the other hand, the small computer offers many advantages. It is at the ready disposal of the user and can in many instances be more readily used in an interactive manner. Trial calculations are less expensive. Graphical output can be obtained with small investment, whereas many mainframe systems do not provide it.

VI. An Example: Start of Magnetron Oscillation

The simulation calculation is demonstrated by starting oscillation from the noise level of computer truncation/round-off error in an eight-digit machine. The magnetron is similar to the 5J26 and the Raytheon QK403. Principal parameters are

N	8	vanes
r_c/r_a	0.4239	normalized cathode radius
f_0	1	normalized π-mode loaded frequency
Q_L	200	π-mode loaded Q
B/B_0	2.5	scaled magnetic field
V_b/V_0	4.3	scaled dc anode voltage

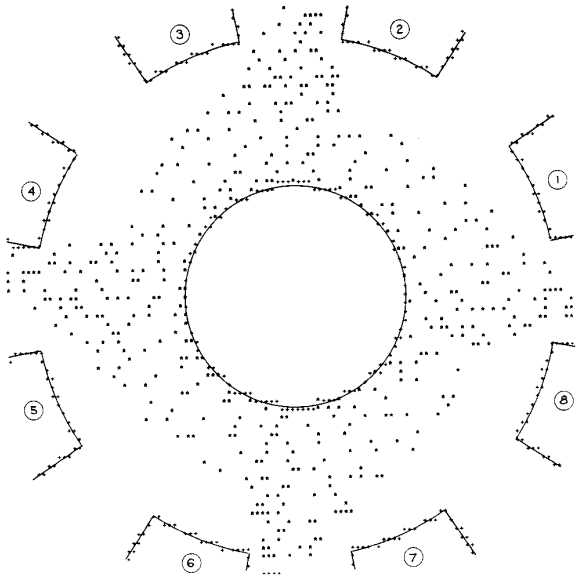

Fig. 4. Printer display of electron stream in the illustrative magnetron simulation at $T = 25.05$.

The RF network is lightly loaded and the magnetic field is somewhat low. These factors facilitate the buildup of oscillation so that a small computer may readily show it. The dc anode voltage is slightly (7.5 percent) higher than the Hartree voltages $V_h/V_0 = 4$.

Fig. 4 is a printer display of the electron cloud after the π mode is well established and steady state is approached. It suffers from paucity (only 500) of electrons and the limitations of the print medium. Computer graphics and video tape technology provide much superior diaplay. The display is in any case limited by the simulation process in that the "electrons" do not have identical amounts of charge.

Fig. 5 shows the effect of the developing electron cloud as it induces charge on the anode after sudden application of the dc anode voltage. The stream at first ($T = 0$ to 10) behaves as in a smooth-anode coaxial diode, its outer limit oscillating at the cyclotron frequency as modified by space-charge effects. This is the "coaxial line" mode; it accounts for the initial RF network energy as shown in Fig. 6. It is seen that the oscillation is a damped one, leading toward the development of a steady-state azimuthally uniform cloud of constant radial extent. During this period there is no appreciable π mode signal, as shown in Fig. 7; this shows a satisfying freedom from noise in the calculation.

After a few RF cycles, the large coaxial mode signal provides, through computer noise, some azimuthally varying signals; these are of the order of -150 db relative to V_0; modes with $k = 1$ to 3 as well as the π mode ($k = 4$) are present. Subsequently ($T > 10$), the π mode is seen to develop from this noise as the π mode bunching of the stream takes place. The π mode potential within the stream is generally higher than the RF anode voltage, indicating its inherent instability. The system energy waveform indicates that the coaxial line mode dies out while the π mode grows. The π mode clearly becomes predominant and, at $T = 18.5$, electrons reach the anode.

Fig. 8 plots the electronic conductance as computed from one-cycle Fourier analysis of the charge waveforms. There has no validity until the π mode is established, at $T > 15$. Thereafter it shows rapid increase as the electron stream forms spokes. Because the RF signal is weak during this formative period and because electrons take a long time to reach the anode, the spokes are wide and heavily laden with charge. They provide substantial electronic current (conductance) during the first rush of collected current ($T = 20$ to 23). Thereafter the spokes become depleted and the electronic current (conductance) is reduced.

As time further increases ($T > 24$), the electronic conductance varies more slowly as the RF signal climbs toward steady state. What appears from this is that while the regime of slowly changing conductance can be considered as a succession of steady states, this does not apply during the initial regime ($T = 0$ to 22).

VII. Conclusion

A procedure for numerical simulation of magnetrons and other crossed-field devices has been described. Factors affecting accuracy and efficiency of computation have been discussed. The minimization of computer "noise" allows the simulation under low RF signal levels, as illustrated in a calculation of magnetron starting.

This simulation program has accuracy and incorporates many details of the anode system of magnetrons and crossed-field amplifiers that must be considered in their analysis. The simulation can thus be used for a quantitative understanding of existing devices, to improve their performance, and to experiment with new configurations. Results of such studies will be presented in forthcoming papers.

Appendix

A. Magnetron RF Network

Fig. 3 shows a portion of the reentrant network of a strapped magnetron having N anodes. The RF potential of the nth anode in the kth mode varies as $\exp(j2\pi kn/N)$.

The elements C_a, G_a, and Γ_a are the only ones active in the $k = 0$ coaxial line mode. They represent energy stored and dissipated in the "end spaces" between the RF anodes and the enclosing magnet faces, the anode–cathode space, and electrical coupling via the cathode/heater connections. These parameters are chosen to reflect the end-space resonance and its Q. Thus, for a unit $k = 0$ mode RF voltage the stored energy W_e determines the capacitance parameter

$$C_a = 2W_e/N.$$

The resonance condition is

$$\Gamma_a = C_a\omega_e^2$$

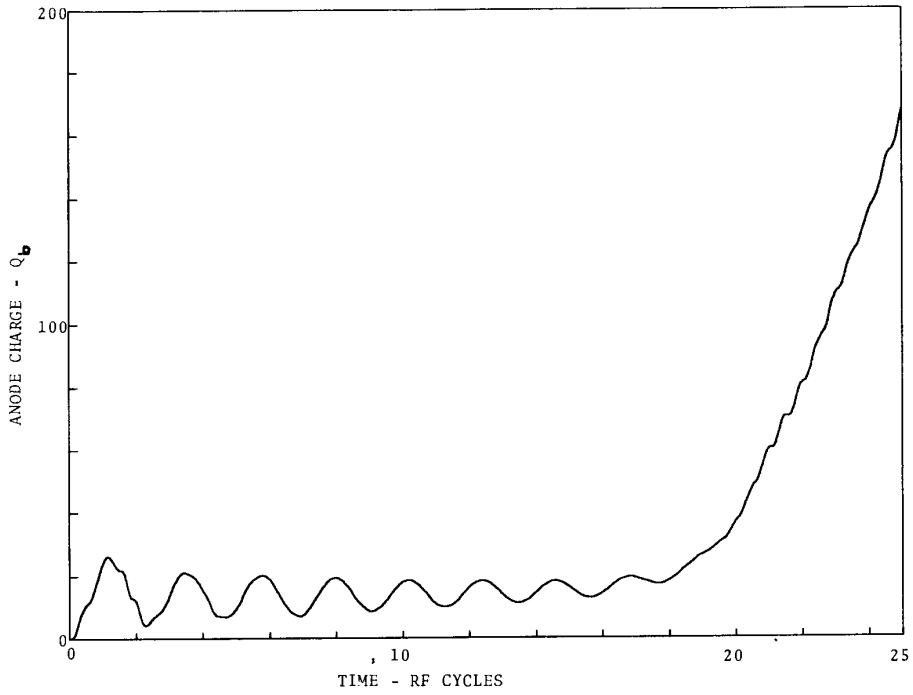

Fig. 5. Total (induced + collected) anode charge.

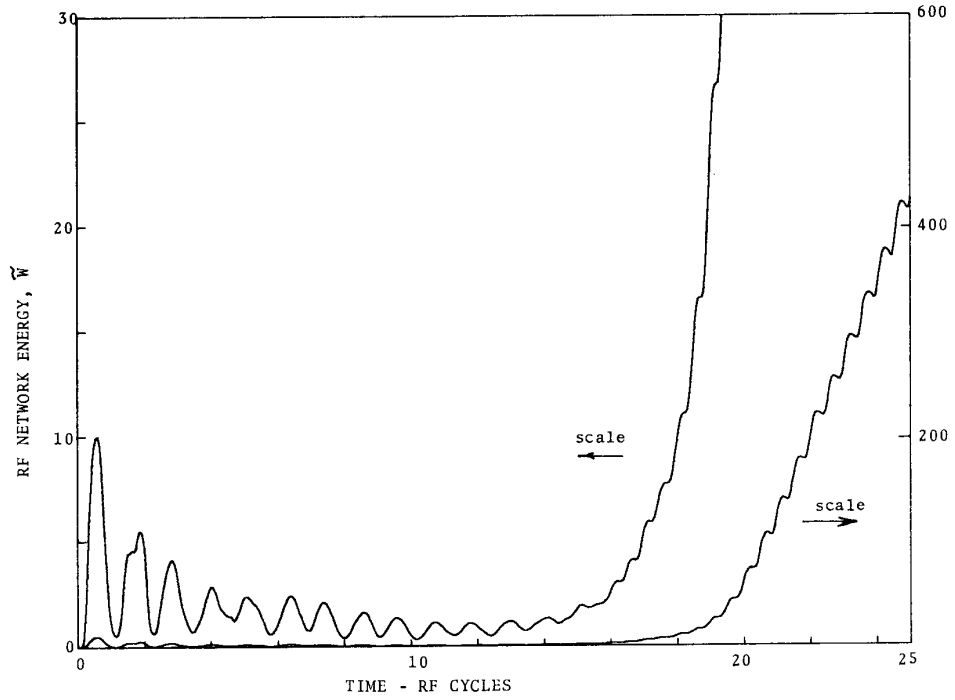

Fig. 6. RF network energy.

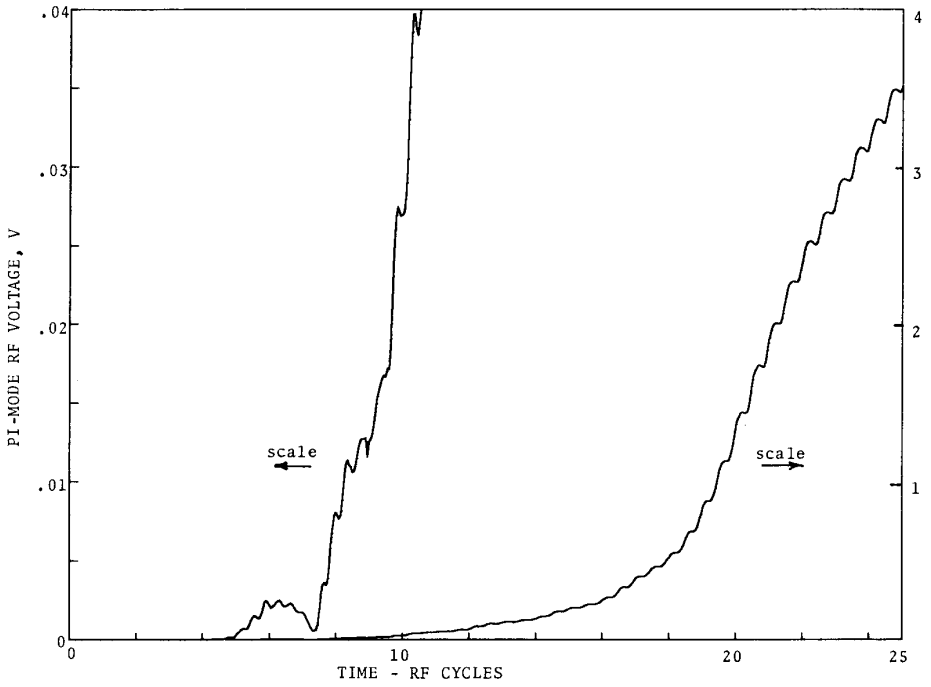

Fig. 7. π mode RF anode voltage.

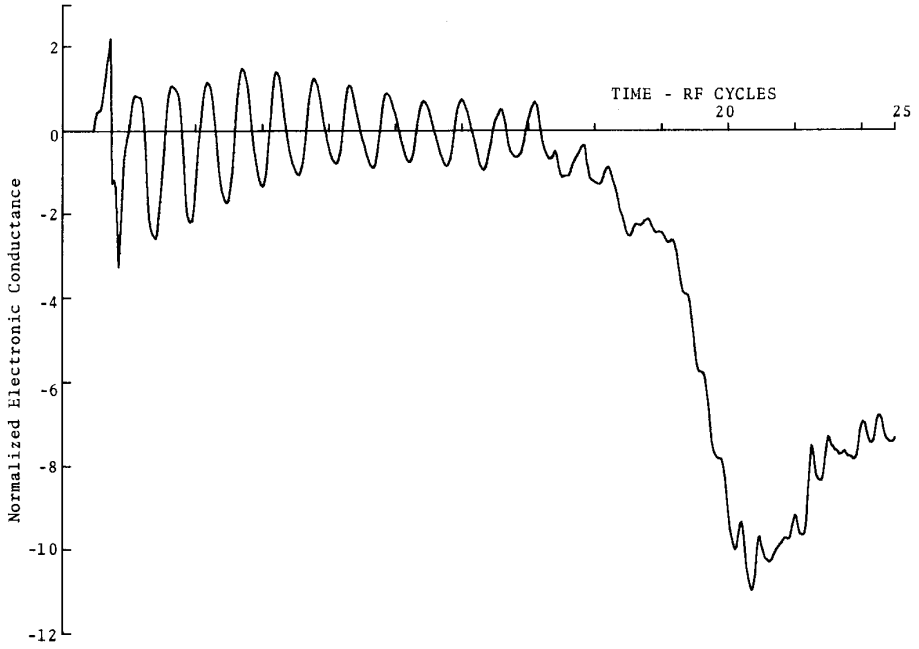

Fig. 8. Electronic conductance. Doubtful meaning until establishment of π mode ($T > 15$).

and the Q requires that

$$G_a = C_a\omega_e/Q_e.$$

In the π mode the energy storage is primarily in the inter-vane space and the dissipation occurs via coupling to the RF load. The parameters C_b, G_b, and Γ_b are determined so that with C_a, G_a, and Γ_a they correctly determine the π mode resonance frequency and Q. The effective π mode parameters being

$$C_\pi = C_b + C_a/4$$

$$\Gamma_\pi = \Gamma_b + \Gamma_a/4$$

$$G_\pi = G_b + G_a/4$$

the π mode energy for a unit RF π mode voltage dictates that

$$C_\pi = 2W_\pi/N$$

$$\Gamma_\pi = C_\pi\omega_\pi^2$$

$$G_\pi = C_\pi\omega_\pi/Q_\pi.$$

Lastly, the strap inductance parameter Γ_c is determined so that with C_a, C_b, Γ_a, and Γ_b the unit cell resonates at the so-called adjacent mode frequency when the network phase shift has the corresponding value

$$C = C_a/4 + C_b(1 - \cos\theta)/2$$

$$\Gamma = \Gamma_a/4 + \Gamma_b(1 - \cos\theta)/2 + \Gamma_c(1 - \cos 2\theta)/2$$

where $\theta = \pi(1 - 2/N)$ is the vane-to-vane phase difference in this mode.

B. Amplitron RF Network

The RF network of Fig. 3 applies to the "Amplitron" form of CFA with the removal of reentrance and introduction of matching networks at input and output. Otherwise, analysis proceeds with the assumption of an RF wave varying along the network as $\exp(j2\pi kn/N)$.

It can be shown that with such an RF wave each node, connected to its neighbors by admittances Y_a, Y_b, and Y_c, behaves as though isolated and endowed with the equivalent admittance

$$Y = Y_a + 2Y_b(1 - \cos\theta) + 2Y_c(1 - \cos 2\theta).$$

The Brillouin diagram can be constructed by assigning the phase θ and calculating the frequency of resonance of this isolated admittance.

As in the magnetron, the $\theta = 0$ mode simply requires resonance of Y_a. The low-frequency edge of the pass band of the network as a high-pass filter is the π mode. This requires resonance of $Y_a + 4Y_b$ and is usually lower than the $\theta = 0$ band edge.

If the number of anodes N is odd (as is customary), π mode amplification is suppressed; RF matching would be impossible at the band edge, anyway. Amplification rather occurs when $N = 2k\pi$, with k the azimuthal mode number. Having determined Y_a and Y_b from the zero and π modes, it simply remains to set the strap inductance parameter Γ_c for resonance at this value of θ.

The π section characteristic admittance of the RF network is

$$Y_{0\pi} = (\Gamma_c/\omega)\sin 2\theta + \omega C_b \sin\theta.$$

This is the value of conductances at anodes #1 and N for match. Capacitances

$$C' = [\Gamma_a/\omega^2 - C_a]/2$$

are also required for match. At anodes #2 and $\#(N-1)$ the required matching admittances are

$$G'' = (\Gamma_c/2\omega)\sin 2\theta$$

$$\Gamma'' = \Gamma_c[1 - \cos 2\theta].$$

REFERENCES

[1] D. R. Hartree, "Method of plotting results of calculations of electron orbits in a magnetron and its application to the determination of the emission, anode current and charge and potential distribution," *Committee for Valve Develop. Rep. Mag.*, vol. 18, 1942.

[2] C. G. Lehr *et al.* Res. Division Tech. Mem. T-347, T-409, T-421; Raytheon Co., Waltham, MA.

[3] S. P. Yu, G. P. Kooyers, and O. Buneman, "Time-dependent computer analysis of electron-wave interaction in crossed fields," *J. Appl. Phys.*, vol. 36, no. 8, 1968.

[4] G. E. Dombrowski and W. C. Price, "Analytic and experimental study of reentrant stream crossed field amplifiers," Final Rep. Contract NAS 3-9710, NASA Lewis Research Center, Cleveland, OH, 1968.

[5] O. Buneman, "A compact non-iterative Poisson solver," SUIPR Rep. 294, Inst. for Plasma Research, Stanford, CA, May 1969.

[6] S. Ramo, "Currents induced by electron motion," *Proc. IRE*, vol. 27, pp. 584–585, Sept. 1939.

*

George E. Dombrowski was born in Bayonne, NJ, on February 22, 1927. He received the B.E.E. degree from The Cooper Union in 1949 and the M.S.E. and Ph.D. degrees from the University of Michigan in 1950 and 1958, respectively, all in electrical engineering.

His professional career encompassed engineering positions at the U.S. Naval Research Laboratory (1948), Raytheon Mfg. Co. (1950), Sperry Gyroscope Corp., and Raytheon Co. (1957–1961). He was at the University of Connecticut (1961–1979) as a Professor of Electrical Engineering and Computer Science. He continues in retirement as a consulting engineer.